Journal of Colloid and Interface Science 676 (2024) 715–725

Contents lists available at ScienceDirect

Journal of Colloid And Interface Science

journal homepage: www.elsevier.com/locate/jcis

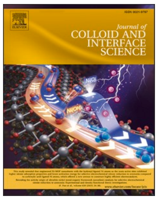

Regular Article

Small-molecule organic electrode materials on carbon-coated aluminum foil for high-performance sodium-ion batteries

Jintao Zou [a], Lijun Ji [d], Ting Xu [a], Quan Gou [e], Siyu Fang [a], Ping Xue [a,b,*], Mi Tang [a,*], Chengliang Wang [c], Zhengbang Wang [a,*]

[a] *Ministry of Education Key Laboratory for the Green Preparation and Application of Functional Materials, Hubei Key Laboratory of Polymer Materials, Collaborative Innovation Center for Advanced Organic Chemical Materials Co-constructed by the Province and Ministry, School of Materials Science and Engineering, Hubei University, Wuhan 430062, China*

[b] *School of Pharmacy, Xianning Medical College, Hubei University of Science and Technology, Xianning 437100, China*

[c] *School of Integrated Circuits, School of Optical and Electronic Information, Wuhan National Laboratory for Optoelectronics (WNLO), Huazhong University of Science and Technology, Wuhan 430074, China*

[d] *Department of Physics and Mechanical & Electrical Engineering, Hubei University of Education, Wuhan 430205, China*

[e] *School of Chemistry and Chemical Engineering, Yangtze Normal University, Chongqing, 408100 China*

GRAPHICAL ABSTRACT

The carbon-coated aluminum foil (CCAF) was employed to tune the interactions of organic molecules and current collectors with outstanding sodium storage in sodium ion battery. As expected, THQAP-CCAF electrodes delivered high specific capacity and superior rate performance.

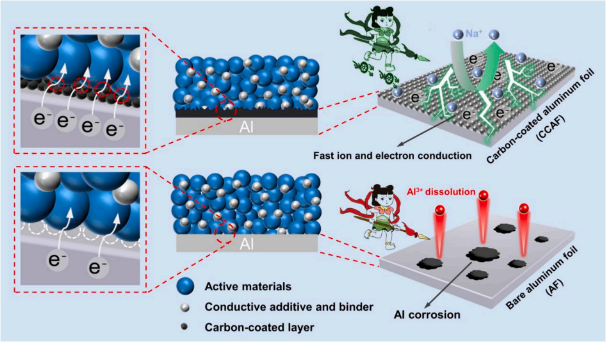

ARTICLE INFO

Keywords:
Organic cathode materials
Carbon-coated aluminum foil
Multiple-weak interactions
Sodium-ion batteries
Quinone compounds

ABSTRACT

Organic molecular electrode materials are promising candidates in batteries. However, direct application of small molecule materials usually suffers from drastic capacity decay and inefficient utilization of active materials because of their high solubility in organic electrolytes and low electrical conductivity. Herein, a simple strategy is found to address the above issues through coating the small-molecule organic materials on a commercialized carbon-coated aluminum foil (CCAF) as the enhanced electrode. Both the experimental and calculation results confirm that the relatively rough carbon coating on the aluminum foil not only exhibits superior adsorption capacity of small-molecule organic electrode materials with a tight contact interface but also provides continuous electronic conduction channels for the facilitated charge transfer and accelerated reaction kinetics. In addition,

---

* Corresponding authors.
E-mail addresses: pingxue@hbust.edu.cn (P. Xue), mtang@hubu.edu.cn (M. Tang), zhengbang.wang@hubu.edu.cn (Z. Wang).

https://doi.org/10.1016/j.jcis.2024.07.170
Received 28 April 2024; Received in revised form 4 July 2024; Accepted 21 July 2024

the carbon coating also inhibits Al corrosion in electrochemical process. As a result, by using the tetrahydroxy quinone-fused aza-phenazine (THQAP) molecule as an example, the THQAP-CCAF electrode exhibits an excellent rate performance with a high capacity of 220 and 180 mAh g^{-1} at 0.1 and 2 A/g, respectively, and also a remarkable cyclability with a capacity retention of 77.3% even after 1700 cycles in sodium-ion batteries. These performances are much more superior than that of batteries with the THQAP on bare aluminum foil (THQAP-AF). This work provides a substantial step in the practical application of the small-molecule organic electrode materials for future sustainable batteries.

1. Introduction

Sodium-ion batteries (SIBs) have attracted extensive attention due to the inexhaustible sodium resources and similar electrochemical properties to lithium-ion batteries, and are considered as a competitive alternative of lithium-ion batteries (LIBs) in the field of large-scale energy storage [1]. However, the radius of sodium ions is inherent larger than that of lithium ions (1.02 Å for Na^+ and 0.76 Å for Li^+), which leads to large volume changes or even pulverization during repeated insertion/extraction of sodium ions in the traditional rigid inorganic electrode materials [2]. This sluggish flaw undoubtedly weakens the stability of the battery. In contrast, more flexible organic materials are adaptive for above challenge to achieve satisfied structural stability. In addition, most organic materials can be sourced directly from renewable resources or prepared from their derivatives without contain heavy metals, which is in line with the concept of green development [3,4]. Therefore, in recent years, organic sodium ion batteries have come to the spotlight and have good application potential in the future grid-scale energy storage.

Benefitting from the precise structure, facile synthetic processes and tunable redox-active sites, organic molecular cathode materials are viewed as one of the most promising candidates for next-generation SIBs [5–8]. However, one of the biggest challenges is that the most of small molecular materials are soluble in liquid organic electrolytes. As a result, almost all small molecule-based electrodes are faced with fast capacity decay and poor rate performances in SIBs [9]. In order to address these problems, many solutions have been proposed, such as introducing strong-ionic bond (for example, salification [7,10–12]), polymerization [13], construction of functional barrier layers [14], the use of high concentration electrolyte or ionic liquid [15,16], carbon-loading [17], and so on [18]. These strategies were effective in improving the electrochemical performance of molecule materials, although more or less lacking in the simplicity or practicability.

Carbon-coated aluminum foil (CCAF) has emerged as an effective current collector because of the advantage on improving the interface contact of cathode materials and foil [19]. It has shown several intrinsically unique merits such as helping to improve battery energy density, inhibiting polarization, reducing internal resistance, increasing cycling stability, and improving electrode materials processing performance. The basic fundamentals are that the carbon coating can make the current collector more uniform concavo-convex surface, reduce the internal resistance, and increase the contact area between the electrode active materials and the current collector. Also, it helps to enhance the adhesion between the active material and the current collector, and thus improve the long cycle performance [20,21]. Because of the above advantages, CCAF is widely used in power lithium-ion batteries. For example, $LiFePO_4$ or NCM based LIBs assembling with CCAF have been extensively studied and well commercialized [22,23]. However, there is little work reported on the effect of CCAF on the electrochemical properties of organic electrode materials, especially the organic sodium ion batteries, and relevant studies are also very lacking [24].

Most organic molecular materials have rich functional groups, such as carbonyl, carboxyl, hydroxyl, amino, etc [9]. Conjugated molecule materials also have π-π interaction. Additionally, carbon materials are normally featured with defects, such as the heteroatoms (O, N and so on), and some functional groups (such as hydroxyl, amino, carbonyl, etc.) [25]. Based on these, we assume that if the CCAF is introduced into the organics electrodes, in addition to the above advantages, the weak intermolecular interactions between the defects of carbon materials on the surface of CCAF and the functional groups of organic molecules may help to improve the cyclability of the organic molecular materials, as shown in Fig. 1. Furthermore, this similar strategy has shown positive results in Li-S batteries [24]. That is, utilizing weak intermolecular interactions between carbon materials and polysulfides have been well investigated to inhibit the shuttle of polysulfides and accelerate their transformation, thereby enhancing the electrochemical performance of Li-S batteries. To verify this hypothesis, we synthesized hydroxyl-contained organic molecule-the tetrahydroxy quinone-fused aza-phenazine (THQAP) as a proof-of-concept cathode material. The effects of CCAF and bare aluminum foil (AF) on the performances of sodium-ion batteries were throughly studied, respectively. Combining with a series of experiments and DFT theoretical calculation, the internal mechanism was also described in details.

2. Experimental section

2.1. Materials

Potassium phthalimide, p-chloranil, 2,5-dihydroxy-1,4-benzoquinone (DHBQ, AR, >99 %), acetic acid (AR, >99.8 %), pyrene-4,5,9,10-tetraone (PTO, AR, >97 %), hydrazine hydrate (AR, >99.8 %), acetonitrile (AR, >99.8 %) were purchased from commercial sources. All reagents and solvents were used without further purification. 1 M $NaPF_6$ in DME were bought from DoDoChem. The preparation of 2,3,5,6-tetraamino-1,4-benzoquinon (TABQ) was based on the previous literature [26].

2.2. Synthesis of 1,2,8,9-tetrahydroxy-5,7,12,14-tetraaza-6,13-pentacenequinone (THQAP)

TABQ (0.168 g, 1 mmol), DHBQ (0.7 g, 5 mmol) and acetic acid (10 mL) were added into a round-bottom flask, and then the mixture was refluxed at 140 °C for 72 h under Ar. After cooling down to room temperature, the black reaction mixture was filtered, washed with HCl, water, hot MeOH and acetone until the filtrate was clear, and then dried in vacuum at 80 °C overnight to yield the product as a black powder. The synthesis route of THQAP was shown in Figure S1. ^{1}H NMR (400 MHz, DMSO-d_6): δ (ppm) 11.44 (s, 4H), 7.50 (s, 4H).

2.3. Synthesis of 2,3-diamino-7,8-dihydroxyphenazine-1,4-dione (QAP)

In a round-bottom flask, a mixture of 2,5-dihydroxy-1,4-benzoquinone (0.2 g, 1.43 mmol) and 2,3,5,6-tetraamino-1,4-benzoquinone (0.24 g, 1.43 mmol) in acetic acid (10 mL) was refluxed at 120 °C for 24 h. After cooling to room temperature, the black reaction mixture was filtered, washed with water, MeOH, and acetone until the filtrate was clear, and dried in vacuum at 90 °C overnight to yield the product as a black powder. The synthesis route of QAP was shown in Figure S2.

2.4. Characterizations

The ^{1}H nuclear magnetic resonance (NMR) spectrums were determined by Bruker AVANCE NEO 400 M spectrometer. X-ray diffraction (XRD) measurements were performed on the Bruker D8 with a Cu Kα radiation (40 KV, 40 mA, λ = 1.5418 Å). The Scanning electron microscopy (SEM) images were performed by Sigma 500. The Fourier transformed infrared spectroscopy (FT-IR) spectrums were determined by Thermo Fisher Nicolet iS50 using the KBr pallet technique. Raman spectrums were recorded on LabRAM HR evolution spectrometer with an excitation source of 532 nm (10 % laser power). The X-ray photoelectron spectroscopy (XPS) were obtained by Thermo SCIENTIFIC ESCALAB 250Xi using monochromatic Al Kα (1486.7 eV) X-rays. UV–Vis absorption spectrums were collected on UV-3600 (Shimadzu, Japan).

2.5. Electrochemical measurements

All the cathodes consisted of 60 wt% THQAP/QAP composite, 30 wt % Ketjen black, and 10 wt% PVDF. The mass of active material was around 0.8–1 mg cm^{-2}. The standard CR2032-type coin cells were assembled in Ar-filled glove box with water and oxygen level under 0.1 ppm, in which the separator was glass fiber filter paper (Whatman), the counter electrode was Na metal, and the electrolyte was 1 M $NaPF_6$ in DME. The Neware (Shenzhen, China) was used as a battery testing system to carry out the electrochemical test, the cut-off potentials were set to 1.0–3.6 V. Cyclic voltammetry (CV) measurements were tested in electrochemical work station (Autolab PGSTAT302N, Switzerland Metrohm) with the voltage range of 1.0–3.6 V. Electrochemical impedance spectroscopy (EIS) were obtained over the frequency range from 100 kHz to 0.1 Hz on electrochemical work station (Autolab PGSTAT302N, Switzerland Metrohm). The chemical diffusion coefficient of Na^+ was tested by galvanostatic intermittent titration technique (GITT) at a current density of 0.05 A/g for 10 min followed by 30 min of relaxation. Where τ was the relaxation time(S), nM and VM were the mass (mol) and molar volume (cm^3 mol^{-1}) of the active material, S was the interfacial area of the electrode (cm^2), ΔEs was the difference between the steady-state potentials before and after a current pulse and thus indicates the change in the potential due to thermodynamics, and ΔEt was the magnitude of the potential changes (without the IR drop) during the current pulse.

$$\boldsymbol{D} = \frac{4}{\boldsymbol{\pi\tau}}\left(\frac{\boldsymbol{n_M V_M}}{\boldsymbol{S}}\right)^2\left(\frac{\boldsymbol{\Delta E_s}}{\boldsymbol{\Delta E_t}}\right)^2$$

2.6. Computational details

The structural models of THQAP, DME, graphite, the complexes THQAP···DME(I), THQAP···DME(II), THQAP…graphite (π···π), THQAP···graphite (C—H···π) and THQAP···graphite (O—H···N) were constructed, and their geometry optimizations were carried out using the self-consistent charge density-functional tight-binding (SCC-DFTB) [27] method with a dispersion correction using the DFTB + program [27,28], the smart algorithm [29] with the force convergence tolerance of 0.05 kcal/mol/Å is used and the SCC tolerance is set to be 1.0×10^{-5} electrons. The interaction energy (i.e., ΔE) of the complex is calculated as the energy difference between the total energy of the complex and the sum of energies of its components.

3. Results and discussion

π-Conjugated quinone small molecules as a type of electrode materials have attracted increasing attention, which can be used as cathode materials for sodium ion batteries [6,30,31]. In order to enhance the interaction between molecule materials and carbon layer, it is necessary to introduce appropriate functional groups into the molecule structure. Therefore, tetrahydroxy quinone-fused aza-phenazine (THQAP), a conjugated carbonyl cathode material containing a large π-conjugated system, as well as four hydroxyl groups and four nitrogen atoms, was selected as the model molecule to study the effect of CCAF on the electrochemical properties of molecule materials. According to the reference [26], the THQAP was synthesized as black powder (details were shown in Supporting Information). The ^1H NMR, infrared spectra and high resolution mass spectrum of the black powder were consistent with those in the literature (Figure S3-5), indicating that THQAP was successfully synthesized.

The scanning electron microscopy (SEM) images of the surface and cross section morphology of CCAF and bare AF were shown in Fig. 2. The surface of bare AF was smooth and flat without obvious impurities (Fig. 2a). The main content was aluminum oxide Al_2O_3. As shown in Fig. 2b, there were spherical and relatively uniform carbon materials on the surface of CCAF. The CCAF surface was further confirmed by XRD and Raman as shown in Figure S6. The CCAF showed a sharp diffraction peak at about 26.5°, which can be assigned to the (002) planes of hexagonal graphite structure [32]. There was no this peak in AF

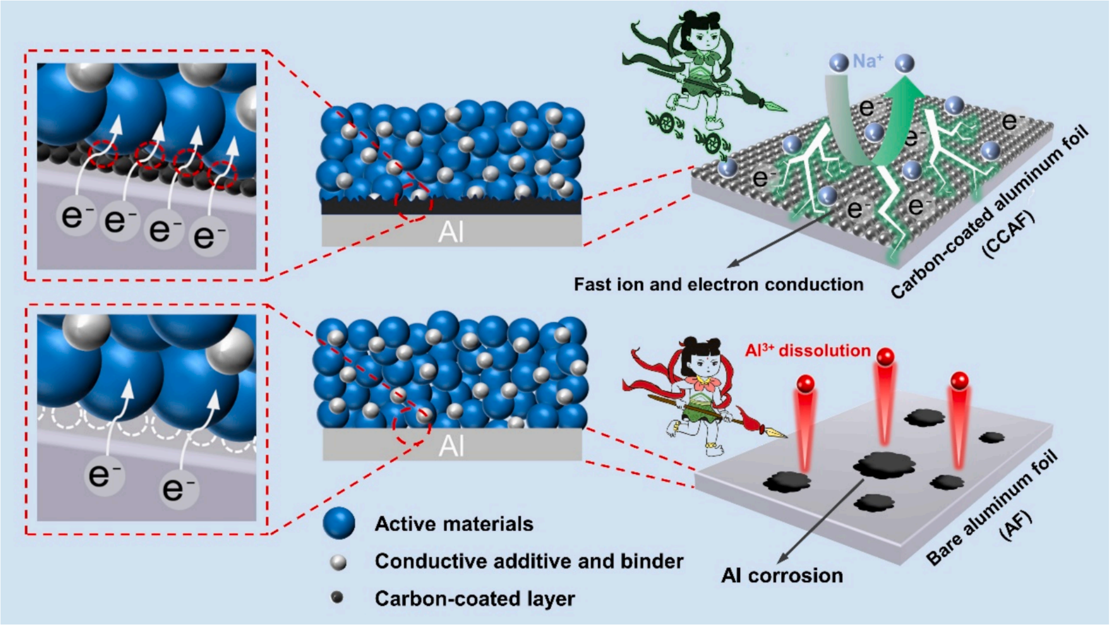

Fig. 1. The faster transport efficiency of ion and electron as well as better anti-corrosion of carbon-coated aluminum foil cathode.

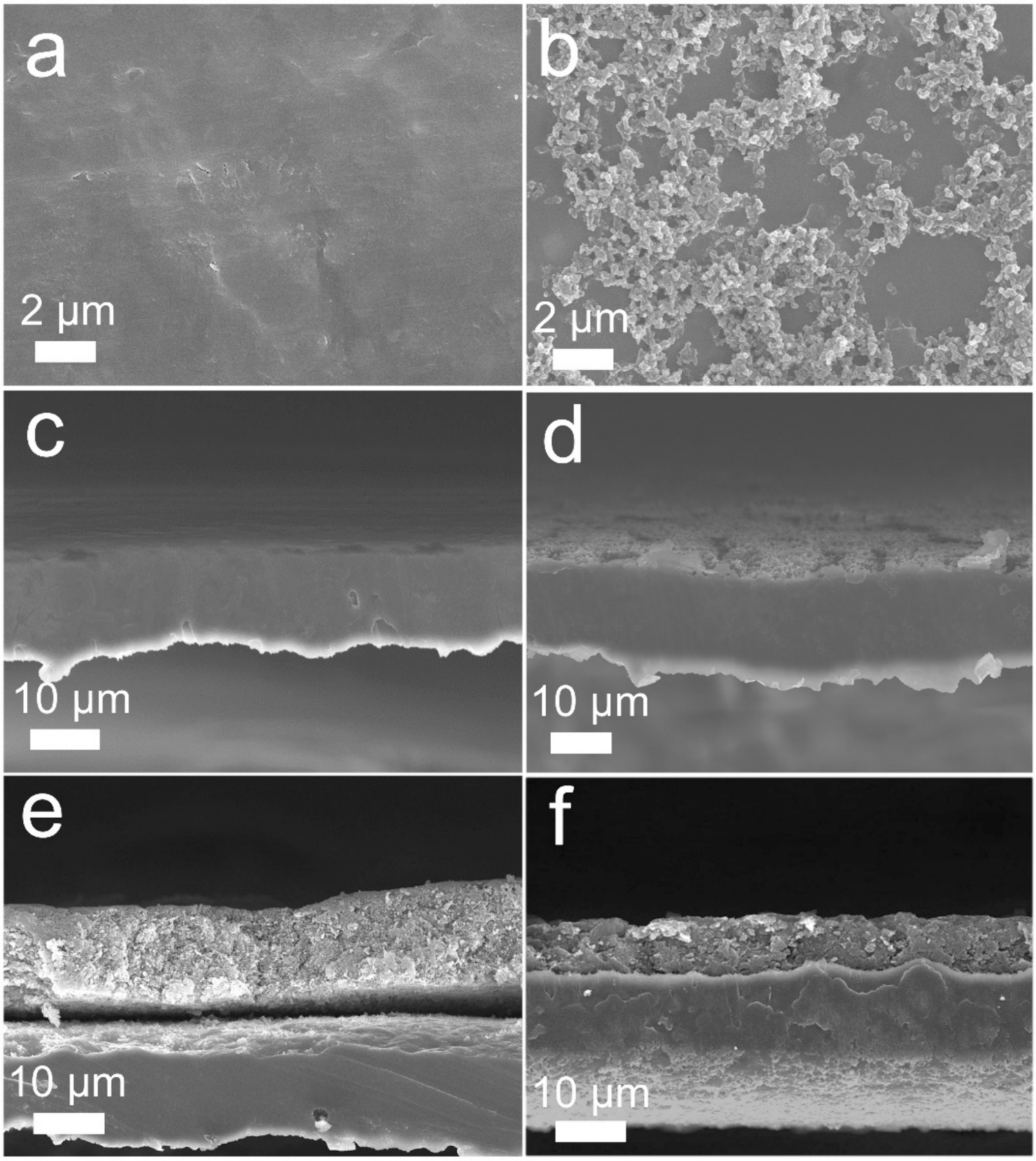

Fig. 2. SEM images of CCAF/AF surface and cross section. (a) The surface of AF. (b) The surface of CCAF. (c) The cross section of AF. (d) The cross section of CCAF. (e) The cross section of THQAP-AF electrode. (f) The cross section of THQAP-CCAF electrode.

(Figure S6a). In addition, it also displayed the characteristic diffraction peaks of Al was at 2θ = 38.5° corresponding to the (1 1 1) plane. This result proved that the carbon was coated on the Al foil surface forming CCAF. The Raman spectra of CCAF also show the characteristic D band (1353 cm^{-1}) and G band (1594 cm^{-1}), corresponding to sp^3 and sp^2 carbon, respectively (Figure S6b). The peak area of the D-band is significantly higher than that of the G-band, indicating that the carbon coated on the Al surface contains a large amount of amorphous carbon [33,34]. In view of the cross section, the bare AF section was uniform (Fig. 2c) while the CCAF presented rough and porous morphology with a thickness of around 2 μm carbon layer on the surface (Fig. 2d and Figure S7). The carbon layer was tightly bound to the surface of the aluminum foil.

Firstly, the obtained material was evenly mixed with the conductive additive KB and PVDF at the weight ratio of 6:3:1, and then coated on the CCAF and bare AF with the same thickness, respectively. Two types of electrodes were prepared after drying at 80 °C under vacuum. The neat THQAP powder was an irregular lamellar like shape (Figure S8). After mixing, THQAP cathodes on the two different foils were of similar morphologies (Figure S9). THQAP was fully wrapped by KB without agglomeration, indicating that the material was uniformly dispersed on both kinds of current collectors. In contrast, the cross-section view of two electrodes showed significant differences. As shown in Fig. 2e, THQAP cathode on the bare AF has intermittent gap between the bottom surface of the active material mixture layer and the top surface of foil. This will undisputedly impair the electrons transfer between the active material and the collector, thus reducing the material utilization ratio. Compared with bare AF, the THQAP cathode on CCAF has more continuous and closer contact with the surface of the aluminum foil without visible interstice, as shown in Fig. 2f. This differentiation has also been observed in $LiFePO_4$- and $LiCoO_2$-based LIBs [35,36]. Moreover, as shown in Figure S10, the adhesion of the electrode film on the surface of CCAF reached ISO 1 level, while it was only ISO 5 level on the bare AF. This result further suggested that the CCAF could offer a stronger interface contact. Generally, the surface of bare AF was covered with an extremely thin layer of Al_2O_3. The low conductivity feature of Al_2O_3 and the intermittent gap implied that there was a lack of a high efficiency conductive network between the THQAP cathode sheet and the aluminum foil for fast electron transfer. For CCAF, the even concave-convex carbon-coated layer could embed the organic molecule and carbon particles into each other. Thus, this tightly bonding the active substance with CCAF greatly reduced interstice, which formed a stronger conductive bridge and network [19,20]. Therefore, we can reasonably infer that compared with bare AF, CCAF would benefit the improvement of the conductivity of THQAP electrode. As shown in Figure S11, the conductivity of THQAP-CCAF and THQAP-AF were 5.6 × 10^3 S m^{-1} and 3.3 × 10^3 S m^{-1}, respectively.

The improved conductivity of the electrode can also reduce the internal resistance of the battery. As shown in the Fig. 3a, the coin-type batteries of two electrodes showed the similar ohmic impedance at room temperature. However, the charge transfer impedance of the CCAF electrode was much smaller than that of bare AF. CCAF was 30 Ω and bare AF was 220 Ω. This suggested that CCAF could effectively reduce the internal resistance of cell and promote interfacial charge transfer. In addition, after the batteries was fully cooled to 0 ℃, both of the ohmic impedance and charge transfer impedance of the two cells increased. It should be noted that the charge transfer impedance of the CCAF based cell was relatively small, reconfirming that less transfer resistance for sodium ions and charge. Finally, the specific surface area of the CCAF cathode electrode was 4.2 m^2 g^{-1}, which was larger than that of the bare AF electrode 3.3 m^2 g^{-1}, as shown in Fig. 3b. The larger specific surface area possibly originated from the pristine porous (Figure S12 and S13)

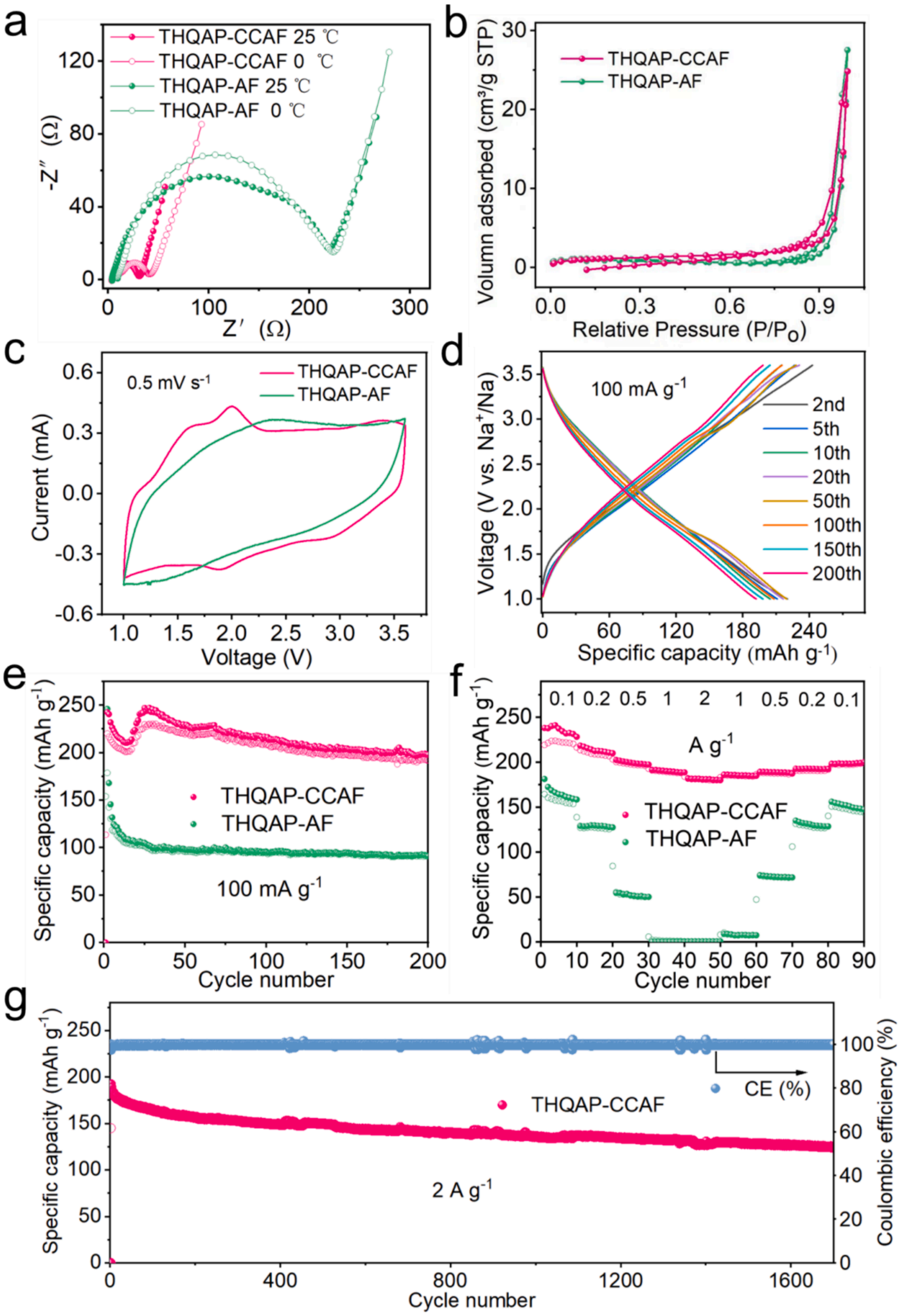

Fig. 3. Sodium-ion batteries performance of THQAP-CCAF and THQAP-AF electrodes. (a) Nyquist plots of THQAP-CCAF and THQAP-AF electrodes at different temperature. (b) N_2 adsorption–desorption isotherms of CCAF and AF electrodes. (c) CV curves of THQAP-CCAF and THQAP-AF at a scan rate of 0.5 mV s^{-1}. (d) Galvanostatic charge–discharge curves of THQAP-CCAF electrodes at a current density of 100 mA/g. (e) Long cycling performances at a current density of 100 mA/g. (f) Rate performances at various current densities from 0.1 to 2 A/g. (g) Long cycling performances at a current density of 2 A/g.

and even concave-convex carbon-coated layer, therefore increasing the contact area between the electrolyte and the electrodes. In a word, the CCAF could act as a good conductive network between the cathode and the collector, which improved the conductivity of the electrodes and reduced the interface charge transfer impedance. All of these preliminary results implied that the battery assembled with CCAF would have favorable rate capability.

Subsequently, we contrastively investigated the performance of sodium-ion batteries with two different electrodes. SIBs were assembled with 1.0 M $NaPF_6$ as electrolytes and sodium foil as counter electrodes. All battery performances were tested at room temperature. The theoretical specific capacity of THQAP is 285 mAh g^{-1} based on the four-electron transfer process. As shown in Fig. 3c, the cyclic voltammetry (CV) showed good reversible curves with broad reduction peaks and anodic peaks between 1.0 V and 3.6 V, which concurred with the curves of galvanostatic cycles (Fig. 3d and Figure S14). There are two pairs of obvious redox peaks at 1.6/1.8 V and 2.0/2.9 V, corresponding to the redox reactions of C═N and C═O. However, the CV curve of THQAP-AF electrode showed no obvious a redox peak because of relatively low conductivity and dissolution of the active material (Figure S14). The average discharge plateau was about 1.8 V with a charging plateau at 2.0 V. Both the charging/discharging platforms and peaks of CV were similar with the reported literature [26], indicating that the electrochemical process of THQAP was not influenced by the CCAF. As shown in Fig. 3e, at a current density of 100 mA/g, the initial capacity of the THQAP cathode on CCAF (THQAP-CCAF) was 222 mAh g^{-1}, reaching 77.9 % of the theoretical specific capacity. There were fewer differences between the first discharge curve and the following curves possibly because of the activation process and low open circuit voltage as shown in Figure S15. The capacity of THQAP-CCAF electrode still remained 199 mAh g^{-1} after 200 cycles with the capacity retention of 89.6 %. It is important to point out that the THQAP-CCAF electrodes suffer from capacity fading in the first dozens of cycles possibly due to incomplete redox reaction of THQAP in the corresponding cycling rounds and a possible activation process [37–39]. As a contrast, the specific capacity of the THQAP cathode on bare AF decayed rapidly after reaching 168 mAh g^{-1}, and further decreased to 91 mAh g^{-1} after 200 cycles, with only the capacity retention of 54.1 %. Zhu *et al.* pointed out that THAQP was soluble in ether and ester electrolyte [26]. Therefore, the decay of capacity on bare AF may be ascribed to the dissolution of the material. However, why the capacity of batteries assembled with CCAF degraded slowly and the capacity retention was even comparable to that of solid electrolytes would be discussed in detail later.

As described above, good electron conduction and lower interface charge transfer impedance made the CCAF-based cells might have better rate performances. As shown in Fig. 3f, at current densities of 0.1, 0.2, 0.5, 1.0, 2.0 A/g, the specific capacities of the CCAF battery were 222, 209 , 196, 188, 180 mAh g^{-1}, respectively. There were similar charging/discharging platforms at different current densities (Figure S16). When a current density was reduced to 0.1 A/g, the battery could also cycle for 10 cycles with a reversible specific capacity of 197 mAh g^{-1}. Under the same current densities, the specific capacities of bare AF battery were only 164, 128, 50, 1, 0.5 mAh g^{-1}, respectively. However, there was no obvious charging/discharging platform at different current densities (Figure S17). Especially, at a high current density of 2 A/g, the bare AF battery given only niggardly capacity while the capacity of the THQAP-CCAF battery could reach 183 mAh g^{-1} with a clear charge/discharge plateau (Figure S18). Furthermore, the THQAP-CCAF cell could deliver a capacity of 195 mAh g^{-1} and a capacity retention of 77.3 % after 1700 cycles at a current density of 2.0 A/g, indicating good rate performance by using CCAF (Fig. 3g). The above results fully showed that the application of CCAF could effectively improve the stability and rate performance of small organic molecules in liquid organic electrolyte.

To get further insight into the reason why the HQAP-CCAF electrode exhibited good stability in liquid organic electrolyte, we further studied the possible weak intermolecular interactions between THQAP molecule and CCAF by Raman spectra and XPS. Firstly, Raman of the pure THQAP molecule was shown in Figure S19. The peak of 2851 cm^{-1} was the stretching vibration of aromatic C—H [40]. The two peaks with wavenumbers of 1670 cm^{-1} and 1465 cm^{-1} were correspond to the asymmetric stretching vibration and the symmetric stretching vibration carbonyl C═O, respectively [41]. The stretching vibrations of C═N were located at 1597 and 1427 cm^{-1}[42]. The peak at around 1504.9 cm^{-1} corresponded to the stretching vibrations of aromatic ring C═C (1344 cm^{-1}) was the in-plane stretching vibration of C—O [43]. 1259 and 1210.9 cm^{-1} were attributed to the in-plane bending vibration of phenolic hydroxyl group [40,44]. Afterwards, THQAP solution in NMP was coated on CCAF and then was dried in vacuum to form THQAP-CCAF composite film. As shown in Fig. 4a the Raman spectra of film revealed that the asymmetric stretching vibration of C═O, stretching vibrations of C═N and C—H B_{2g} mode peak all abnormally shifted toward the direction of high wave number (blue shift). The wavenumbers of C═O in THQAP-CCAF composite film migrated to 1690 cm^{-1} with a sharp blue shift of 20 cm^{-1} comparing with pure THQAP. This phenomenon illustrated that there was improper hydrogen-bonded complexes between C═O or C═N and the surface functional groups of the carbon material in the CCAF [45]. If C═O···H—O type H-bond was formed, it would weaken the carbonyl bond and lower C═O stretching wavenumbers, that is, the red shift [46,47]. The blue shift of C═O wavenumber indirectly suggested the strengthening of the C═O bond. We speculated that the lone pair electrons of heteroatoms in C═O or C═N groups from THQAP could serve as proton-acceptors to form C—H···O═C/N═C type H-bond with sp^2 C—H of carbon from CCAF. As a result, a small amount of electron cloud density was transferred from O or N atoms in THQAP to sp^2 C—H of carbon in CCAF, resulting in increased bond strength of C═O with the contraction of the bond lengths, thus giving blue shift [45]. Meanwhile, upon complex formation, C—H of carbon material was elongated slightly corresponding red shift. As shown in Figure S20, the band of carbon sp^2 C—H in coated-carbon aluminum foil was about 2940 cm^{-1}. After being coated with THQAP molecule, it moved to 2920 cm^{-1}, that is, a red shift of 20 cm^{-1}. This significant red shift strongly indicated the existence of the above interaction. This weak interaction contributed to inhibiting the dissolution of THQAP in the organic electrolyte and enhancing the adhesion between the molecular material and CCAF.

Secondly, as shown in Figure S21, the stretching vibrations of THQAP aromatic C—H also showed a certain degree of red shift as well as the significant enhancement of peak intensity. $\Delta\nu(C - H)$ was 10 cm^{-1} for stretching vibration. We speculated that the C—H red shift and peak enhancement might arise from the formation of intermolecular C—H···π interaction (so-called C—H···π type H-bond) between the C—H of THQAP molecular and large π system of carbon material [45,48]. Furthermore, the interaction between hydroxyl groups of THQAP and carbon was also evaluated. As shown in Fig. 4a, the wavenumber of in-plane bending vibration of hydroxyl plane at 1210.9 cm^{-1} showed a small red shift, only about 6 cm^{-1} Raman shift, while the peak intensity was slightly increased. The results implied a formation of intermolecular complex or weak forces. One feature was common to all generally accepted carbon materials of which there were few defects (containing O, N, or other functional groups) in the structure or the surface [25], which acted as proton acceptor (Y). Thus, it was suggested that the formation of O—H···Y contacts played a key role in above complex or weak forces, accounting for this Raman red shift [49]. In a word, all of above weak forces together contributed to the stability of THQAP molecular material in the electrolyte and enhanced adhesion.

On the other hand, the interactions between the THQAP molecules and the CCAF were investigated by XPS. As shown in Fig. 4b, the XPS N 1 s spectrum of THQAP molecule displayed two peaks at 398.6 and 400.0 eV, which represent the signals of C═N and C—N [26]. After coating the THQAP molecule on CCAF, also called as THQAP-CCAF composite film, the N 1 s could also be fitted into two peaks at 399.5

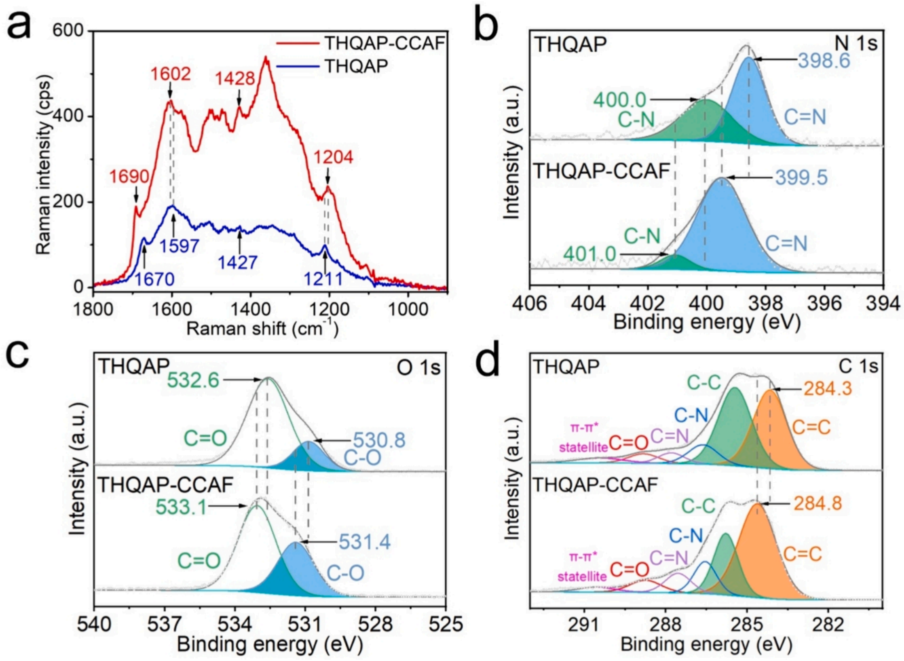

Fig. 4. (a) Raman spectrums of THQAP molecule and THQAP-CCAF. (b-d) High-resolution XPS spectrums of (b) N 1 s, (c) O 1 s and (d) C 1 s, respectively.

and 401.0 eV. The binding energy of C═N and C—N were shifted by 0.9 eV and 1.0 eV towards higher binding energy, respectively. The intensity of C—N bond decreased significantly, while the intensity of C═N bond increased. These suggested the conversion of C—N to C═N and electron transfer process from N to the CCAF, resulting in the N atom more electropositive [50]. That is to say, there was the interactions between the C═N of THQAP and CCAF.

Furthermore, a similar phenomenon was also found in the XPS spectrums of O 1 s. As shown in Fig. 4c, THQAP molecule displayed two peaks at 530.8 and 532.6 eV, which represented the signals of C—O and C═O [26]. Both of them were shifted to the high binding energy in the THQAP-CCAF composite film, locating at 531.4 and 533.1 eV respectively. It implied that electrons were transferred from O to CCAF [51]. The high-resolution XPS spectrum of C 1 s in Fig. 4d and Figure S22 could be exactly deconvoluted into six peaks, including C═C (284.3 eV), C—C (285.4 eV), C—N (286.6 eV), C═N (287.8 eV), C═O (288.8 eV) and a satellite peak (290.4 eV), respectively [26]. In the THQAP-CCAF composite film, C—C bond was shifted to high binding energy owing to interactions between THQAP molecule and carbon on CCAF. The suppression of 285.4 eV-peak and the intensified of 284.3 eV-peak implied enhanced π-π stacking between THQAP molecule and carbon on CCAF [52].

It is precisely because of the above-mentioned weak forces that THQAP molecular interacted with two kinds of carbon to form a sandwich structure interaction, which confined the molecular material sandwich layer. Thus, the interactions between THQAP and solvent molecules were weakened and the dissolution was inhibited. The UV spectrum of the THQAP cathodes in electrolyte solution further confirmed better stability of CCAF electrode than that of bare AF. After 15 days, THQAP was almost undetectable in CCAF-based electrode while high concentrations of THQAP were detected with bare AF (Figure S23). By the way, that the UV spectrum of THQAP-CCAF and THQAP-AF on one day was different from that on other days possibly was related to the test-used solvents. After soaking THQAP-CCAF and THQAP-AF in the DME electrolyte for one day, both of them were associated with polar solvent DME. Therefore, the π-π* band of THQAP UV peak showed a red shift [53,54]. When it reached the saturation, the peak shape kept relatively stable. Therefore, the UV spectrum of THQAP-CCAF and THQAP-AF showed stable peaks in the following days. UV spectrum of THQAP in DME for different days after by soaking CCAF and AF films also confirmed that CCAF had stronger adsorption of THQAP molecule. After three days, the absorption peak of the CCAF-soaked solution decreased significantly compared with the initial state, while the decrease of AF absorption peak was not obvious (Fig. 5a). This result showed that CCAF can effectively adsorb THQAP molecules and inhibit its dissolution in the electrolyte (Fig. 5b). To better understand this competitive force, we calculated the corresponding binding energies by DFT. Four phenolic hydroxyl groups of THQAP scaffold as the typical hydrogen bond donor could form hydrogen bonds with DME with binding energy of -6.18 kcal mol^{-1} (Fig. 5c). In addition, π-π stacking interactions between π-conjugated system of THQAP and π system of carbon materials (CCAF) showed the binding energy of -48.55 kcal mol^{-1} (Fig. 5d). The C—H···π interactions between C—H bond of THQAP and π system of carbon as well as O—H···Y hydrogen bonds between O—H groups of THQAP and few heteroatoms of carbon showed the binding energy of -20.66 kcal mol^{-1} and -19.36 kcal mol^{-1}, respectively (Figure S24, S25). It was clear that the interaction forces between THQAP and CCAF was significantly stronger than that of THQAP and DME in terms of binding energy. Therefore, THQAP was preferentially adsorbed on carbon materials rather than dissolved in DME, and thus the CCAF electrode has better stability in the electrolyte.

In addition to the weak interaction, the corrosion of the collector during the electrochemical process was also crucial to the lifespan of batteries [55]. It was shown that the CCAF as a superior current collector featured corrosion inhibition characteristics was widely used in power LIB [56]. Generally, CCAF could effectively protect the current collector from being corroded by the electrolyte and minimize the side reactions [16]. As depicted in Fig. 6, morphological changes of the Al surface were surveyed. After 100 cycles, obvious cracks (Fig. 6c) and pits structure could be observed on the surface of bare AF (Fig. 6a), while the surface of CCAF (Fig. 6b still retained a regular carbon-coated layer (Fig. 6d). The conductive network possibly was damaged if the aluminum foil was corroded, resulting in poor cycle performances. The coated carbon layer on the surface of aluminum foil acted as a protective coating against corrosion and excessive side reactions with the electrolyte at high potential, thus helping to maintain a complete conductive network and good cycle stability. In order to further examine decomposition

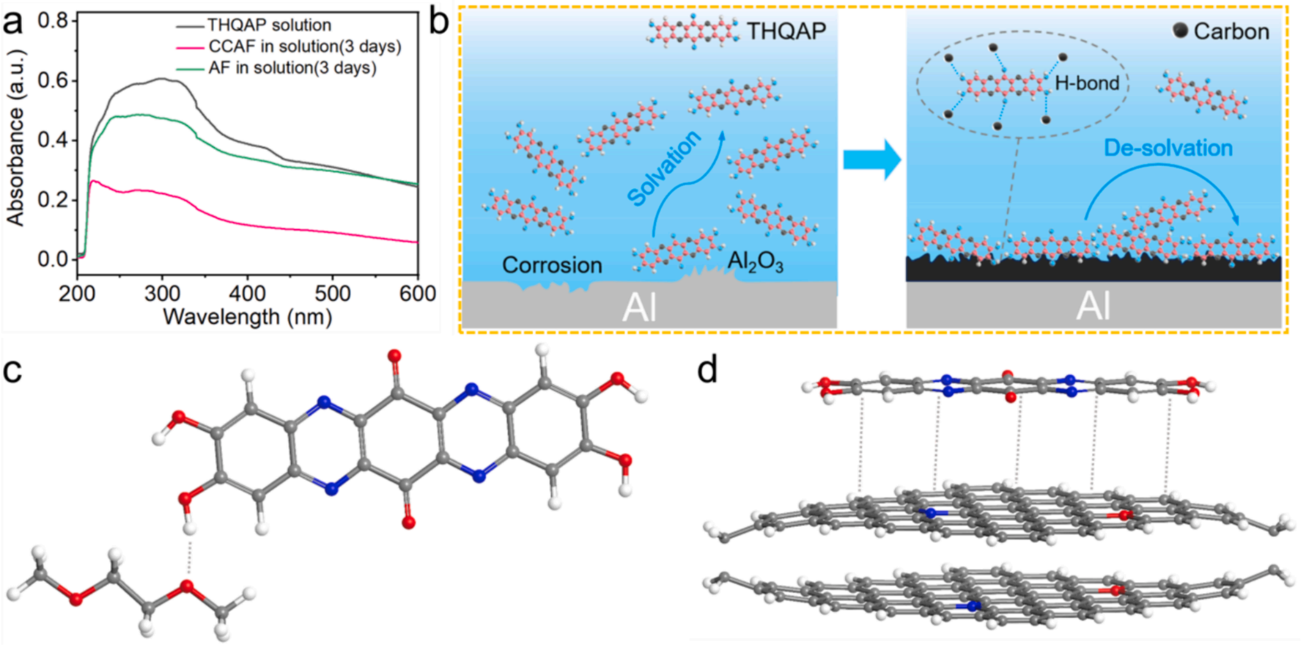

Fig. 5. The interactions between THQAP and CCAF or AF. (a) UV spectrum of THQAP in DME for different days after by soaking CCAF and AF films. (b) Schematic illustration of the adsorption of THQAP by pristine AF and CCAF. Theoretical calculations and simulations. (c) The interactions between THQAP and DME electrolyte. (d) The π-π stacking interactions between THQAP and carbon materials (CCAF).

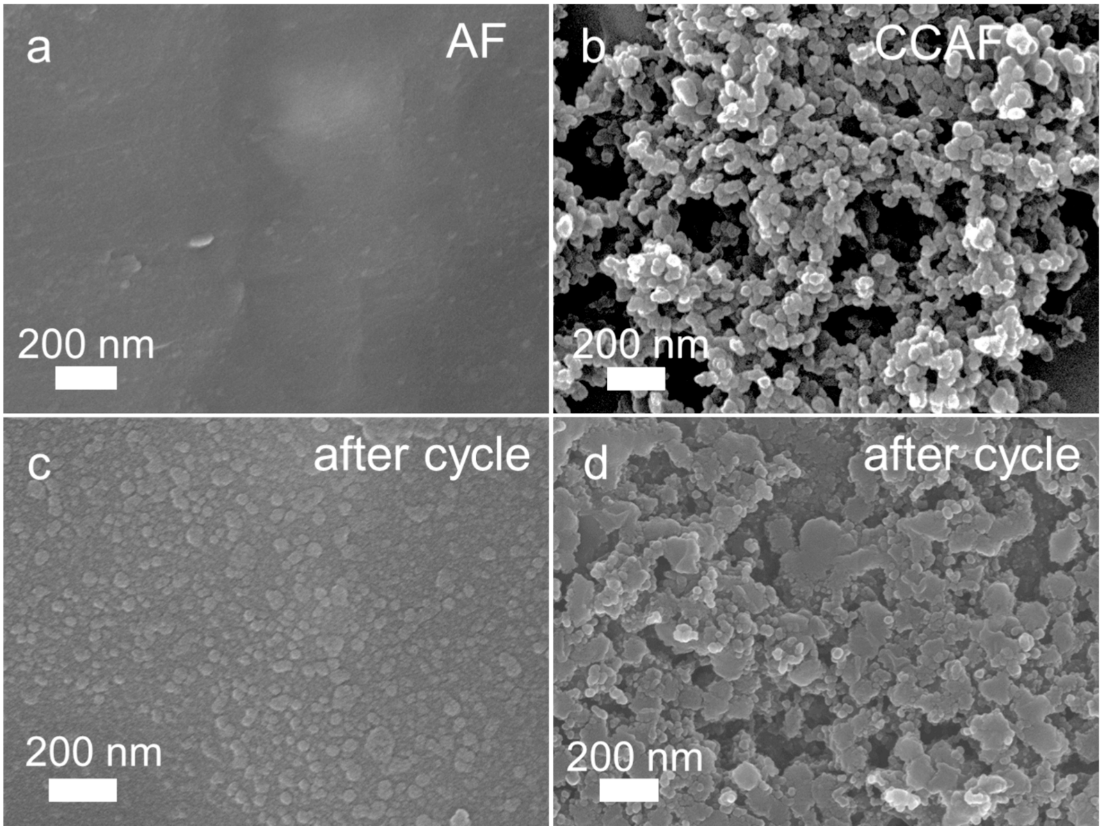

Fig. 6. The SEM images of the pristine (a) AF and (b) CCAF. SEM images of (c) THQAP-AF electrode and (d) THQAP-AF electrode after 100 cycles.

products, the electrolyte compositions of cycled batteries assembled with different aluminum foil were analyzed by ICP-OES. It was worthy noted that the concentration of Al^{3+} in the electrolyte of CCAF cell was only about 5.1 mg/L, which was significantly lower than that of bare AF (20 mg/L) (Figure S26). Lower Al content straightforward revealed the less dissolution or corrosion of aluminum foil. The above results fully proved that coated-carbon aluminum foil has a positive contribution in inhibiting aluminum foil corrosion and reducing side reactions in the electrochemical process, and plays an important role in the cycle performances of the battery.

To gain insight into the above weak interaction, we further investigated the effect of CCAF on other organic small molecule materials. Two different types of molecule materials were chosen as the model, namely QAP containing both amino and hydroxyl groups, and pyrene-4,5,9,10-tetraone (PTO) without other functional groups except for carbonyls. Based on the above analysis, it was quite reasonable to suppose that there were similar interactions between CCAF and QAP because of similar molecule structure of QAP with THQAP. However, this interaction may be weak in situation of pyrene-4,5,9,10-tetraone because it lacked the necessary functional groups. Therefore, as predicted, the performances of the two types of molecule materials may be significantly different. As shown in Fig. 7a and Fig. 7b, at a current density of 100 mA/g, the stable specific capacity of QAP cell assembled with CCAF (QAP-CCAF) reached 206 mAh g^{-1} over 450 cycles with an average voltage of about 2.2 V. By comparison, the QAP cell assembled with AF (QAP-AF) showed obvious capacity decay with the capacity retention of 72.7 % (133 mAh g^{-1}) after 450 cycles. However, whether using CCAF or AF, the capacity of PTO electrodes deteriorated rapidly (Fig. 7c). At current densities of 0.1, 0.2, 0.5, 1.0 and 2.0 A/g, the QAP-CCAF electrode also showed excellent rate capability with 257, 235, 227, 220 and 210 mAh g^{-1}, respectively (Fig. 7d). When the current density was decreased to 0.1 A/g, the battery continued to retain stable cycling performance with the capacity retention of 90.3 % (232 mAh g^{-1}). Meanwhile, the QAP-AF electrode exhibited relatively poor rate performance. In contrast, PTO electrode showed almost no capacity at 1.0 A/g (Figure S27). Finally, the long-term cycling stability of QAP-CCAF electrode at a high current density was shown in Figure S28. At 2.0 A/g, the QAP-CCAF electrode delivered an initial high capacity of 210 mAh g^{-1}, which was retained at 188 mAh g^{-1} even after 280 cycles with a capacity retention of 89.5 %. These electrochemical performances are superior to that of all the previously reported small molecule materials for SIBs (Table S1). All these results once again strongly demonstrated that the interactions between CCAF and organic molecule materials enhanced the molecular structure stability in the organic electrolyte and thus contributed to the high rate performance and cyclability.

Finally, we also analyzed the electrochemical kinetics and Na^+ ion diffusion coefficient of the THQAP electrode in two different batteries. The CV curves at different scan rates and the galvanostatic intermittent titration technique (GITT) were measured, respectively (Figure S29-S32). As shown in Figure S33, the THQAP electrode with coated-carbon aluminum foil was dominated by the capacitive effect and the ion diffusion coefficient was 5.5×10^{-11} cm s^{-1}, which together facilitated the high rate performance. The electrode with bare AF was more inclined to the capacitance process, and the ion diffusion coefficient was relatively small (1.5×10^{-11} cm s^{-1}). Therefore, the capacitive effect combined with the higher ion diffusion coefficient again suggested that the batteries with coated-carbon aluminum foil have better rate performance, especially the rapid charge and discharge ability.

4. Conclusions

In conclusion, we propose a novel and practical strategy to enhance the sodium storage of molecule materials by using the carbon-coated aluminum foil (CCAF) as a functional current collector. Based on the interactions between carbons of CCAF and molecules, organic molecules CCAF electrodes showed noticeable superiority in interface contact, adhesion force with electrode materials, the interface charge transfer impedance and specific surface area comparing with the bare aluminum foil (AF). In addition, it also exhibited the effective corrosion inhibition and weakening side reactions of electrolyte during the charging and discharging process in SIBs. Accordingly, as a proof-of-concept, THQAP-CCAF electrodes showed excellent cyclability and rate performance. Specifically, the THQAP-CCAF electrode gave a stable capacity of 192 mAh g^{-1} at 0.1 A/g for 200 cycles, while the THQAP-AF electrode only delivered a capacity of 92 mAh g^{-1} after 200 cycles. Even at a current density of 2.0 A/g, the capacity of THQAP-CCAF electrode still

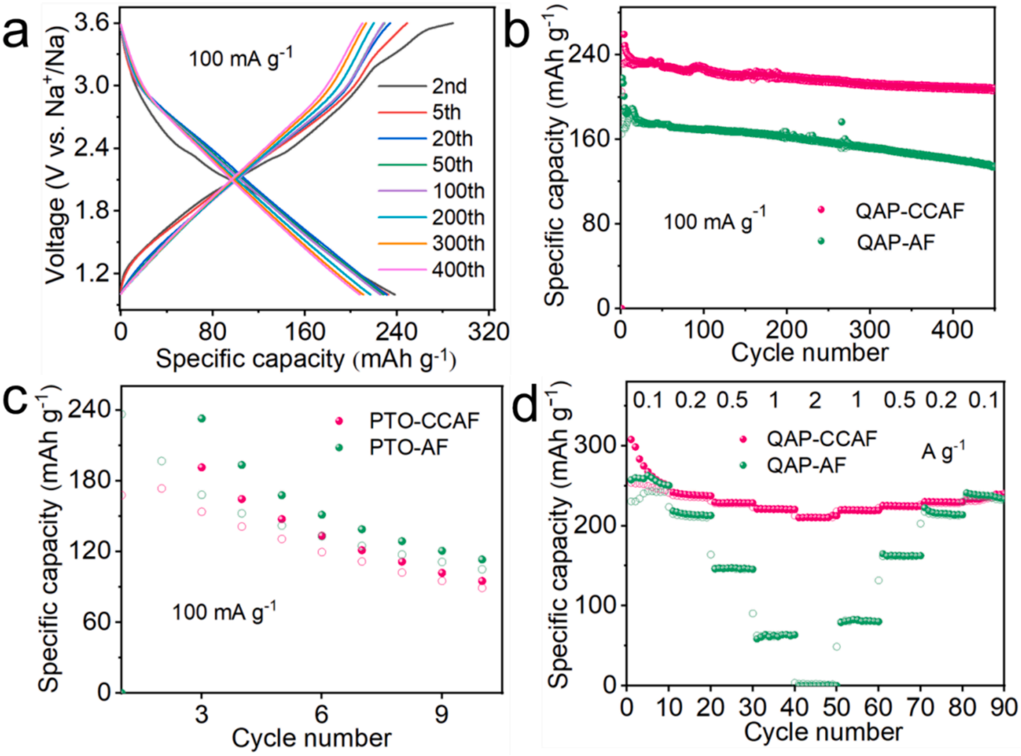

Fig. 7. (a) Galvanostatic charge–discharge curves of QAP-CCAF electrodes at a current density of 100 mA/g. (b) Long cycling performances at a current density of 100 mA/g for QAP-CCAF and QAP-AF electrodes. (c) Cycling performances of PTO-CCAF and PTO-AF electrodes at a current density of 100 mA/g. (d) Rate performances at various current densities from 0.1 to 2 A/g for QAP-CCAF and QAP-AF electrodes.

maintained at 125 mAh g^{-1} after 1700 cycles, while the bare AF electrode showed fast degradation. These results were comparable with that of performances in solid-state electrolytes batteries [26] and ionic liquid electrolyte-basaed organic sodium-ion batteries [16]. The stable cycling performance was ascribed to the formation of weak interactions, such as π-π interaction, C—H···π and O—H···Y types of H-bond between THQAP and carbon materials of CCAF. The DFT calculation showed these multi-type interactions were stronger than that of between THQAP and DME solvent molecules, which contributed a pivotal role in inhibiting dissolution of molecular materials in organic electrolyte and maintaining the long-term cyclability of batteries. Additionally, the significant differences of QAP and PTO battery performances also verified the key role of the above-mentioned weak interactions. Our work confirms that applying CCAF is a practical, handy and effective method to improve the electrochemical properties of organic small molecule electrode materials, and provides deep insights into the enhanced electrochemical performances by the interactions between CCAF and molecules. We believe it will arouse extensive interest in using organic cathode materials for future practical applications, and other functional electrode molecules were also investigated.

CRediT authorship contribution statement

Jintao Zou: Writing – original draft, Investigation, Data curation. **Lijun Ji:** Investigation, Data curation. **Ting Xu:** Investigation. **Quan Gou:** Investigation. **Siyu Fang:** Investigation. **Ping Xue:** Supervision, Investigation. **Mi Tang:** Project administration, Investigation. **Chengliang Wang:** Investigation. **Zhengbang Wang:** Investigation.

Declaration of competing interest

The authors declare that they have no known competing financial interests or personal relationships that could have appeared to influence the work reported in this paper.

Data availability

No data was used for the research described in the article.

Acknowledgments

This work was supported by National Natural Science Foundation of China (Grant No. 22278116 and 12105091), China Postdoctoral Science Foundation (2022M710849 and 2023T160137), Department of Education of Hubei Province (Q20221004) and Overseas Expertise Introduction Center for Discipline Innovation (D18025). The authors thank Hubei Provincial Natural Science Foundation of China (Project No. 2024AFB1016 and 2023AFB479).

Appendix A. Supplementary material

Supplementary data to this article can be found online at https://doi.org/10.1016/j.jcis.2024.07.170.

References

[1] R. Usiskin, Y. Lu, J. Popovic, M. Law, P. Balaya, Y.-S. Hu, J. Maier, Fundamentals, status and promise of sodium-based batteries, Nat. Rev. Mater. 6 (2021) 1020–1035.

[2] Y. Chen, K. Fan, Y. Gao, C. Wang, Challenges and perspectives of organic multivalent metal-ion batteries, Adv. Mater. 34 (2022) 2200662.

[3] Y. Lu, J. Chen, Prospects of organic electrode materials for practical lithium batteries, Nat. Rev. Chem. 4 (2020) 127–142.

[4] D. Xu, M. Liang, S. Qi, W. Sun, L.-P. Lv, F.-H. Du, B. Wang, S. Chen, Y. Wang, Y. Yu, The progress and prospect of tunable organic molecules for organic lithium-ion batteries, ACS Nano 15 (2021) 47–80.

[5] Y. Wang, P. Bai, B. Li, C. Zhao, Z. Chen, M. Li, H. Su, J. Yang, Y. Xu, Ultralong cycle life organic cathode enabled by ether-based electrolytes for sodium-ion batteries, Adv. Energy Mater. 11 (2021) 2101972.

[6] C. Wang, W. Tang, S. Jia, Y. Yan, D. Li, Y. Hu, J. Gao, H. Wu, M. Wang, S. Liu, H. Lai, T. Zou, L. Xu, J. Xiong, C. Fan, Benzene-bridged anthraquinones as a high-rate and long-lifespan organic cathode for advanced Na-ion batteries, Chem. Eng. J. 426 (2021) 131251.

[7] J. Wang, X. Liu, H. Jia, P. Apostol, X. Guo, F. Lucaccioni, X. Zhang, Q. Zhu, C. Morari, J.-F. Gohy, A. Vlad, A high-voltage organic framework for high-performance Na- and K-Ion batteries, ACS Energy Lett. 7 (2022) 668–674.

[8] Y. Hu, Q. Yu, W. Tang, M. Cheng, X. Wang, S. Liu, J. Gao, M. Wang, M. Xiong, J. Hu, C. Liu, T. Zou, C. Fan, Ultra-stable ultra-long-lifespan and ultra-high-rate Na-Ion batteries using small-molecule organic cathodes, Energy Storage Mater. 41 (2021) 738–747.

[9] C. Wang, Weak intermolecular interactions for strengthening organic batteries, Energy Environ. Mater. 3 (2020) 441–452.

[10] T. Ma, L. Liu, J. Wang, Y. Lu, J. Chen, Charge storage mechanism and structural evolution of viologen crystals as the cathode of lithium batteries, Angew. Chem. Int. Ed. 59 (2020) 11533–11539.

[11] W. Tang, R. Liang, D. Li, Q. Yu, J. Hu, B. Cao, C. Fan, Highly stable and high rate-performance Na-Ion batteries using polyanionic anthraquinone as the organic cathode, ChemSusChem 12 (2019) 2181–2185.

[12] C. Zhang, Y. Zhang, K. Fan, Q. Zou, Y. Chen, Y. Wu, S. Bao, L. Zheng, J. Ma, C. Wang, Diradicals or zwitterions: the chemical states of m-benzoquinone and structural variation after storage of Li ions, CCS Chemistry 4 (2021) 2768–2781.

[13] M. Tang, S. Zhu, Z. Liu, C. Jiang, Y. Wu, H. Li, B. Wang, E. Wang, J. Ma, C. Wang, Tailoring π-conjugated systems: from π-π stacking to high-rate-performance organic cathodes, Chem 4 (2018) 2600–2614.

[14] S. Zhu, M. Tang, Y. Wu, Y. Chen, C. Jiang, C. Xia, S. Zhuo, B. Wang, C. Wang, Free-standing protective films for enhancing the cyclability of organic batteries, Sustain. Energ Fuels 3 (2019) 142–147.

[15] J. Yang, Z. Wang, Y. Shi, P. Sun, Y. Xu, Poorly soluble 2,6-dimethoxy-9,10-anthraquinone cathode for lithium-ion batteries: the role of electrolyte concentration, ACS Appl. Mater. Interfaces 12 (2020) 7179–7185.

[16] X. Wang, Z. Shang, A. Yang, Q. Zhang, F. Cheng, D. Jia, J. Chen, Combining quinone cathode and ionic liquid electrolyte for organic sodium-ion batteries, Chem 5 (2019) 364–375.

[17] M. Tang, H. Sun, L. Su, Y. Gao, F. Chen, Z. Wang, C. Wang, Organics-MXene composites as electrode materials for energy storage, Batteries & Supercaps 6 (2023) e202200402.

[18] P. Poizot, J. Gaubicher, S. Renault, L. Dubois, Y. Liang, Y. Yao, Opportunities and challenges for organic electrodes in electrochemical energy storage, Chem. Rev. 120 (2020) 6490–6557.

[19] H. Li, L. Wang, Y. Song, Z. Zhang, H. Zhang, A. Du, X. He, Significance of current collectors for high performance conventional lithium-ion batteries: a review, Adv. Funct. Mater. 33 (2023) 2305515.

[20] H. Jeong, J. Jang, C. Jo, A review on current collector coating methods for next-generation batteries, Chem. Eng. J. 446 (2022) 136860.

[21] L. Hu, J. Deng, Q. Liang, J. Wu, B. Ge, Q. Liu, G. Chen, X. Yu, Engineering current collectors for advanced alkali metal anodes: a review and perspective, EcoMat 5 (2023) e12269.

[22] H.-C. Wu, H.-C. Wu, E. Lee, N.-L. Wu, High-temperature carbon-coated aluminum current collector for enhanced power performance of $LiFePO_4$ electrode of Li-ion batteries, Electrochem. Commun. 12 (2010) 488–491.

[23] R. Wang, W. Li, L. Liu, Y. Qian, F. Liu, M. Chen, Y. Guo, L. Liu, Carbon black/graphene-modified aluminum foil cathode current collectors for lithium ion batteries with enhanced electrochemical performances, J. Electroanal. Chem. 833 (2019) 63–69.

[24] T. Li, H. Bo, H. Cao, Y. Lai, Y. Liu, Carbon-coated Aluminum Foil as Current Collector for Improving the Performance of Lithium Sulfur Batteries, Int. J. Electrochem. Sci. 12 (2017) 3099–3108.

[25] G. Wang, M. Yu, X. Feng, Carbon materials for ion-intercalation involved rechargeable battery technologies, Chem. Soc. Rev. 50 (2021) 2388–2443.

[26] L. Chen, L. Cheng, J. Yu, J. Chu, H.-G. Wang, F. Cui, G. Zhu, Tailored organic cathode material with multi-active site and compatible groups for stable quasi-solid-state lithium-organic batteries, Adv. Funct. Mater. 32 (2022) 2209848.

[27] M. Elstner, D. Porezag, G. Jungnickel, J. Elsner, M. Haugk, T. Frauenheim, S. Suhai, G. Seifert, Self-consistent-charge density-functional tight-binding method for simulations of complex materials properties, Phys. Rev. B 58 (1998) 7260–7268.

[28] M. Elstner, P. Hobza, T. Frauenheim, S. Suhai, E. Kaxiras, Hydrogen bonding and stacking interactions of nucleic acid base pairs: a density-functional-theory based treatment, J. Chem. Phys. 114 (2001) 5149–5155.

[29] M.S. Amer, J.A. Elliott, J.F. Maguire, A.H. Windle, Calculations of the Raman spectra of C60 interacting with water molecules, Chem. Phys. Lett. 411 (2005) 395–398.

[30] B. Häupler, A. Wild, U.S. Schubert, Carbonyls: powerful organic materials for secondary batteries, Adv. Energy Mater. 5 (2015) 1402034.

[31] Y. Wu, R. Zeng, J. Nan, D. Shu, Y. Qiu, S.-L. Chou, Quinone electrode materials for rechargeable lithium/sodium ion batteries, Adv. Energy Mater. 7 (2017) 1700278.

[32] L. Guo, W. Song, C. Xie, X. Zhang, M. Hu, Characterization and thermal properties of carbon-coated aluminum nanopowders prepared by laser-induction complex heating in methane, Mater. Lett. 61 (2007) 3211–3214.

[33] X. Li, S. Deng, M.N. Banis, K. Doyle-Davis, D. Zhang, T. Zhang, J. Yang, R. Divigalpitiya, F. Brandys, R. Li, X. Sun, Suppressing corrosion of aluminum foils via highly conductive graphene-like carbon coating in high-performance lithium-based batteries, ACS Appl. Mater. Interfaces 11 (2019) 32826–32832.

[34] M. Wang, M. Tang, S. Chen, H. Ci, K. Wang, L. Shi, L. Lin, H. Ren, J. Shan, P. Gao, Z. Liu, H. Peng, Graphene-armored aluminum foil with enhanced anticorrosion

performance as current collectors for lithium-ion battery, Adv. Mater. 29 (2017) 1703882.

[35] D.-Y. Shin, D.-H. Park, H.-J. Ahn, Interface modification of an Al current collector for ultrafast lithium-ion batteries, Appl. Surf. Sci. 475 (2019) 519–523.

[36] T. Liu, F. Cao, L. Ren, X. Li, S. Sun, X. Sun, Z. Zang, Q. Niu, J. Wu, A theoretical study of different carbon coatings effect on the depolarization effect and electrochemical performance of LiFePO4 cathode, J. Electroanal. Chem. 807 (2017) 52–58.

[37] X. Sun, W. Si, X. Liu, J. Deng, L. Xi, L. Liu, C. Yan, O.G. Schmidt, Multifunctional Ni/NiO hybrid nanomembranes as anode materials for high-rate Li-ion batteries, Nano Energy 9 (2014) 168–175.

[38] Y. Huang, Z. Xu, J. Mai, T.-K. Lau, X. Lu, Y.-J. Hsu, Y. Chen, A.C. Lee, Y. Hou, Y. S. Meng, Q. Li, Revisiting the origin of cycling enhanced capacity of Fe_3O_4 based nanostructured electrode for lithium ion batteries, Nano Energy 41 (2017) 426–433.

[39] X. Wang, L. Qiao, X. Sun, X. Li, D. Hu, Q. Zhang, D. He, Mesoporous NiO nanosheet networks as high performance anodes for Li ion batteries, J. Mater. Chem. A 1 (2013) 4173–4176.

[40] S.E. Jayaraj, V. Ramakrishnan, Surface-enhanced Raman scattering of 1,5-dihydroxyanthraquinone in silver sol, Spectrochim. Acta, Pt. a: Mol. Biomol. Spectrosc. 51 (1995) 979–983.

[41] P.K. Dutta, J.A. Hutt, Infrared and resonance Raman spectroscopic studies of 1-hydroxy-9,10-anthraquinone and its metal complexes, J. Raman Spectrosc. 18 (1987) 339–344.

[42] A.G. Brolo, D.E. Irish, Raman spectral studies of aqueous acidic pyrazine solutions, Z. Naturforsch., A 50 (1995) 274–282.

[43] S. Ramalingam, S. Periandy, S. Mohan, Vibrational spectroscopy (FTIR and FTRaman) investigation using ab initio (HF) and DFT (B3LYP and B3PW91) analysis on the structure of 2-amino pyridine, Spectrochim. Acta, Pt. A: Mol. Biomol. Spectrosc. 77 (2010) 73–81.

[44] G. Smulevich, L. Angeloni, S. Giovannardi, M.P. Marzocchi, Resonance Raman and polarized light infrared spectra of 1,4-dihydroxyanthraquinone. vibrational studies of the ground and excited electronic states, Chem. Phys. 65 (1982) 313–322.

[45] P. Hobza, Z. Havlas, Blue-shifting hydrogen bonds, Chem. Rev. 100 (2000) 4253–4264.

[46] J. Joseph, E.D. Jemmis, Red-, blue-, or no-shift in hydrogen bonds: a unified explanation, J. Am. Chem. Soc. 129 (2007) 4620–4632.

[47] D. Sajan, I.H. Joe, V.S. Jayakumar, NIR-FT Raman, FT-IR and surface-enhanced Raman scattering spectra of organic nonlinear optic material: p-hydroxy acetophenone, J. Raman Spectrosc. 37 (2006) 508–519.

[48] S. Panda, K. Kundu, S. Umapathy, R.L. Gardas, A combined experimental and theoretical approach to understand the structure and properties of N-methylpyrrolidone-based protic ionic liquids, Chemphyschem 18 (2017) 3416–3428.

[49] P.D. Vaz, P.J.A. Ribeiro-Claro, C—H···O hydrogen bonds in liquid cyclohexanone revealed by the νC-O splitting and the νC–H blue shift, J. Raman Spectrosc. 34 (2003) 863–867.

[50] J.S. Stevens, L.K. Newton, C. Jaye, C.A. Muryn, D.A. Fischer, S.L.M. Schroeder, Proton transfer, hydrogen bonding, and disorder: nitrogen near-edge X-ray absorption fine structure and X-ray photoelectron spectroscopy of bipyridine-acid salts and co-crystals, Cryst. Growth Des. 15 (2015) 1776–1783.

[51] J. He, W. Chen, H. Gao, Y. Chen, L. Zhou, Y. Zou, R. Chen, L. Tao, X. Lu, S. Wang, Tuning hydrogen binding modes within RuO2 lattice by proton and electron co-doping for active and stable acidic oxygen evolution, Chem Catal. 2 (2022) 578–594.

[52] D. Tuncel, A.N. Ökte, Adsorption and photoactivity performances of copper(II)–benzene-1,3,5-tricarboxylate (Cu-BTC) and zeolitic imidazolate framework (ZIF-8): effect of humidity, J. Chem. Technol. Biot. 98 (2023) 2925–2942.

[53] M. Homocianu, Exploring solvatochromism: a comprehensive analysis of research data, Microchem. J. 198 (2024) 110166.

[54] P. Li, J. Hur, Utilization of UV-Vis spectroscopy and related data analyses for dissolved organic matter (DOM) studies: a review, Crit. Rev. Environ. Sci. Tec. 47 (2017) 131–154.

[55] P. Du, D. Liu, X. Chen, H. Xie, X. Qu, D. Wang, H. Yin, Research progress towards the corrosion and protection of electrodes in energy-storage batteries, Energy Storage Mater. 57 (2023) 371–399.

[56] C. Lamiel, I. Hussain, X. Ma, K. Zhang, Properties, functions, and challenges: current collectors, Mater. Today Chem. 26 (2022) 101152.